Archives of Civil and Mechanical Engineering (2024) 24:239
https://doi.org/10.1007/s43452-024-01050-0

ORIGINAL ARTICLE

Microstructural and properties investigations of tantalum-doped tungsten diboride ceramic coatings via HiPIMS and RF magnetron sputtering

Rafał Psiuk[1] · Justyna Chrzanowska-Giżyńska[2] · Piotr Denis[1] · Edyta Wyszkowska[3] · Maria Wiśniewska[4] · Marta Lipińska[5] · Ewa Wojtiuk[6] · Łukasz Kurpaska[3] · Jerzy Smolik[7] · Tomasz Mościcki[1]

Received: 15 April 2024 / Revised: 7 August 2024 / Accepted: 16 September 2024

Abstract

In this work, tantalum-doped tungsten boride ceramic coatings were deposited from a single sputtering target with the radio frequency (RF) and high-power impulse magnetron sputtering (HiPIMS) methods. Two-inch torus targets were synthesised from pure elements with the spark plasma sintering (SPS) method with a stoichiometric composition of $W_{1-x}Ta_xB_{2.5}$ ($x = 0$, 0.08, 0.16, 0.24). Films were deposited with RF and HiPIMS power suppliers at process temperatures from RT to 600 °C. The substrate heating and the energy of the ionised material impacting the substrate increase the surface diffusivity of adatoms and are crucial in the deposition process. The results of SEM and XRD investigations clearly show that the addition of tantalum also changes the microstructure of the deposited films. The coatings without tantalum possess a finer microstructure than those with 24% of tantalum. The structure of films is homogeneous along the film thickness and composed mainly of columns with a (0001) preferred orientation. Deposited coatings are composed mainly of P_6/mmm α-WB_2 structures. The analysis of nanoindentation results allowed us to determine that ceramic coatings obtained with the HiPIMS method possess hardness above 41 GPa and a ratio of hardness to reduced Young modulus above 0.1. The thickness of HiPIMS-deposited films is relatively small: only around 60% of the RF magnetron sputtered coatings even when the average power input was two times higher. However, it has been shown that the RF coatings require heating the substrate above 400 °C to obtain a crystalline structure, while the HiPIMS method allows for a reduction of the substrate temperature to 300 °C.

Keywords RF magnetron sputtering · HiPIMS magnetron sputtering · Superhard ceramic coatings · Transition metal borides · Deposition temperature

✉ Rafał Psiuk
rpsiuk@ippt.pan.pl

✉ Tomasz Mościcki
tmosc@ippt.pan.pl

[1] Institute of Fundamental Technological Research, Polish Academy of Sciences, Pawinskiego 5B, 02-106 Warsaw, Poland

[2] VIGO Photonics, Poznańska 129/133, 05-850 Ożarów Mazowiecki, Poland

[3] NOMATEN Centre of Excellence, National Centre for Nuclear Research, A. Soltana 7, 05-400 Otwock, Poland

[4] Łukasiewicz Research Network—Poznan Institute of Technology, Ewarysta Estkowskiego 6, 61-755 Poznan, Poland

[5] Faculty of Materials Science and Engineering, Warsaw University of Technology, Wołoska 141, 02-507 Warsaw, Poland

[6] Faculty of Mechanical and Industrial Engineering, Warsaw University of Technology, Narbutta 85, 02-524 Warsaw, Poland

[7] Institute for Sustainable Technologies, Łukasiewicz Research Network, ul. Pułaskiego 6/10, 26-600 Radom, Poland

Published online: 28 September 2024

1 Introduction

High hardness, wear resistance, thermal stability and oxidation resistance are required for high-quality protective coatings [1]. Super-hard materials perfectly meet the condition of excellent mechanical properties, but not all of them meet the conditions of thermal and chemical stability. In the last few years, numerous scientific studies have indicated the great potential of transition metal borides as hard [2] and super-hard materials [3]. Particularly high interest may be aroused by tungsten borides doped with transition metals (e.g. rhenium [4], titanium [5], zirconium [6], tantalum [7] or molybdenum [8]) because previous studies have shown that, apart from high hardness and fracture toughness, they may exhibit high thermal stability and resistance to oxidation. Among the previously mentioned additions, tantalum gained our special interest because it enables one to shift the thermally driven decomposition and phase transformation of α-WB_2 (AlB_2-type) to ω-W_2B_5 (W_2B_5-type) to temperatures above 1200 °C [9] and increases oxidation resistance [10]. Pangilinan et al. [11] showed that tantalum satisfies the Hume-Rothery rules and is able to form a substitutional solid solution with WB_2, with solubility limits at less than 10 at.%, and metal atom substitution causes intrinsic hardening. Further increasing tantalum content has an influence on extrinsic hardening through the refinement of grain morphology and the addition of secondary phases (TaB_2 and WB_4). The addition of tantalum causes an increase in the ductility of the obtained material also. Fuger et al. [12] showed that tantalum alloyed WB_2 coatings ($W_{0.93}Ta_{0.07}B_{1.76}$) hold high cracking resistance, $K_{IC} = 3.8 \pm 0.5$ MPa$\sqrt{\text{m}}$, and at the same time are superhard, but also exhibit high compressive stresses (− 1.4 GPa). Several publications report on even higher fracture toughness values for transition metal nitrides, e.g. Seidl et al. [13]; however, such outstanding mechanical properties place tungsten diboride coatings doped with tantalum in the "flexible" and superhard material groups [14], which are simultaneously hard, tough and resistant to cracking in bending.

So far, tungsten boride coatings have been mainly deposited by magnetron sputtering with the following power sources: direct current (DC) [15], RF [16] and HiPIMS [17]. DC magnetron sputtering is usually used in industrial applications due to a high rate of deposition and low prices of power supplies. However, non-conductive materials cannot be deposited by DC sputtering since the non-conductive coating on the substrate prevents electron flow through the anode. Additionally, this method possesses other disadvantages like low plasma energy and a low metal ionisation rate, which cause weak film/substrate adhesion [18] and high residual compressive stresses [12] in coatings due mainly to argon bombardment [19]. During DC MS deposition of transition metal borides, heating of the substrate is needed to increase the adatoms mobility and obtain crystalline coatings. Usually, during the deposition process with DC power supplies, the energy is used to heat the entire vacuum station instead of being used in sputtering sources as well as for densification of the film. Fuger et al. [12, 15], during deposition of $W_{1-x}Ta_xB_{2-z}$ with DC MS, heated up the chamber to the deposition temperatures (T_{dep}) of 700 °C and 500 °C to obtain the substrate temperatures of 400 °C and 300 °C respectively. Of course, the problem grows with the increase in the mass of the details with which the surface needs to be coated. The solution is the use of power supplies that enable the achievement of higher energy in the plasma plume, thus higher ionisation and, consequently, activation of thermal surface diffusion and film densification [20]. A higher degree of ionisation can be obtained during RF-MS deposition [21]. In the case of tungsten borides, using this method allows for α-WB to be obtained at 530 °C [22], while DC-deposited films at 700 °C (other conditions were similar) are composed mainly of the β-WB polymorph [23], which is much softer than α-phase [24].

In RF sputtering, charge build-up on insulating targets is avoided by changing the sign of the anode–cathode polarisation at a high rate (commonly 13.56 MHz). The RF power is applied continuously, which results in a low-density plasma similar to DCMS. In the case of HiPIMS magnetron sputtering, short pulses are used, and the charge accumulation is thought to be compensated by the opposite charge when the applied voltage is switched off or reversed for a brief moment [25]. As a result of peak power densities of several kilowatts per square centimetre, a dense ionised plasma is obtained and incident irradiation at the growing film surface is dominated by metal-gas ions, while the amount of gas ions is lower. Such conditions allow for a decrease in the ion-induced residual stress in deposited layers [19]. Additionally, due to the fact that the ionised target particles reaching the substrate have a similar mass to the film-forming species, a more effective momentum transfer is obtained and the recoil density and energy needed to reduce porosity at low deposition temperatures are provided [26].

The type of power source used to create the plasma significantly impacts the properties of the coating that is deposited. In this paper, we analyse the properties of tantalum-doped tungsten borides and investigate the effects of the sputtering method on the coating properties. In previous studies, $W_{1-x}Ta_xB_{2-z}$ coatings were deposited with the DC MS method from two sources. Therefore, the study of this material deposited with HiPIMS and RF magnetron will complement the transition metal doped tungsten boride coatings database and promote their applications in various engineering fields. We also aim to determine the

effects of substrate temperature on the deposited coatings, which would be interesting for both temperature-sensitive substrates and large-size elements, as well as because of the energetic efficiency of the process. Additionally, we will simplify the deposition process by sputtering from a single target.

2 Materials and methods

2.1 Deposition process

In this work, sputtering targets were prepared using the spark plasma sintering (SPS) process. Tungsten (99.9% purity, average grain size – 25 µm, Sigma Aldrich), tantalum (99.8% purity, average grain size – 250–350 µm, Sigma Aldrich), and amorphous boron (95% purity, average grain size – 1 µm, Sigma Aldrich) powders in a (W + Ta)/B molar ratio of 1/2.5 were mixed for 30 min using a Turbula® T2F shaker-mixer (WAB, Switzerland). Afterward, the received material was placed in the sintering chamber of an HP D 25/3 furnace (FCT Systeme, Germany) for the sintering process. Detailed information on the manufacturing process is described in the literature [27].

The deposition process was performed in a vacuum chamber that was pumped down to a base pressure of $4 \cdot 10^{-6}$ mbar and then filled with argon to a working pressure of $9 \cdot 10^{-3}$ mbar (0.9 Pa). A two-inch diameter $W_{1-x}Ta_xB_{2.5}$ (x = 0, 0.08, 0.16, 0.24) target was mounted on the sputtering cathode of a magnetron module (PREVAC MS2 63C1) with an RF or HiPIMS power supply. The pulse parameters are the result of an optimisation process, which looked at the coating stoichiometry, mechanical properties and deposition rate [17]. The pulse duration and pulse frequency were 20 µs and 700 Hz, respectively. No bias voltage was applied to the substrate.

Sputtered material was deposited on a Si (100) substrate (ITME, Poland) and placed in front of the magnetron cathode 80 mm from its surface. Before sputtering, the substrate's surface was plasma cleaned by applying – 800 V bias voltage for 15 min. During deposition, the substrate was heated to a temperature in the range of 200–600 °C. The resistive substrate heater (refractory metal module with a silicon carbide-coated graphite (SiCg) heating element) was placed on the backside of the substrate. The distance from the heater to the substrate was 1 cm. The surface temperature was calibrated with a pyrometer. Each deposition process lasted 90 min.

2.1.1 Deposition rate

To deposit at least a 1.5 µm thick coating, the deposition rate at different process parameters was tested using a quartz crystal thickness monitor inserted in the place of the substrate. It is well known that the deposition rate during the HiPIMS process is much lower than during RF-MS [28]. Therefore, the deposition parameters were selected so that the deposition rate would be similar. In Fig. 1, the comparison of deposition rate as a function of the average deposition power for both methods is shown.

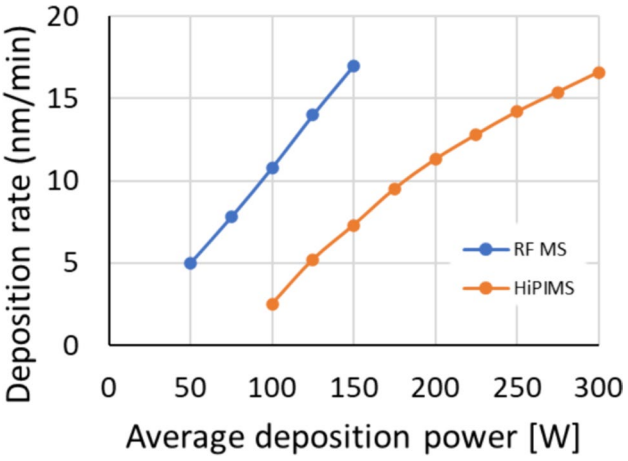

Fig. 1 Deposition rates at different sputtering powers. The target to substrate distance was 80 mm; HiPIMS pulse frequency, 700 Hz; pulse time duration, 20 µs; target, $W_{0.92}Ta_{0.08}B_{2.5}$

Table 1 The roughness and thickness of coatings deposited at different substrate temperatures (T_s)

T_s (°C)	RF	HiPIMS	RF	HiPIMS
	Film thickness (µm)		Roughness Ra (nm)	
200	–	1.1	–	1.1
300	1.89	1.28	3.7	1.3
400	1.95	1.19	3.5	1.3
500	1.87	1.12	2.5	1.6
600	1.65	–	1.8	–

In the case of the RF power supply, the power was changed from 50 to 150 W during deposition rate estimation and set at 150 W during coating deposition, with a different Ta amount and at elevated substrate temperatures. It should be noted that the measurement was impossible above 150 W due to instabilities on the quartz crystal. For the HiPIMS power supply, the pulse duration and pulse frequency were 20 µs and 700 Hz, respectively, and the average power was changed from 100 to 300 W during deposition rate measurements and set to 250 W during the processes.

Each deposition process lasted 90 min and resulted in 1.1–1.9 µm coating thickness. As is shown in Table 1, Sect. 3.4, the deposition rates obtained from film thickness measurements deposited with HiPIMS is lower than those

from quartz crystal thickness monitor. This is the result of the substrate heating and the use of theoretical parameters, such as the speed of sound and the density of undoped WB_2.

2.2 Characterisation

The surface's microstructure, cross-section (fracture of the specimen) and thickness of deposited films were investigated using a scanning electron microscope (SEM, JSM-6010PLUS/LV JEOL microscope, Akishima, Japan). The chemical composition was determined using an energy dispersive X-ray spectroscope (EDS) with an accelerating voltage of 7 kV. The analysis of light elements, such as boron, especially in the presence of heavy elements, is subject to significant measurement error. Therefore, before measuring the deposited coatings, we calibrated the EDS detector with a commercial W_2B_5 standard with a purity of 99.9% (TYR Material, China). The coating's thickness was measured on the basis of a cross section of deposited films.

X-ray diffractometry (XRD) was carried out using a Bruker D8 Discover in 2θ scan mode, with Cu-Kα radiation ($\lambda = 1.5418$ Å). Measurements were taken with an incidence angle fixed at an 8° position to diminish the signal from the substrate while maintaining a high intensity of the signal originating from the coating [4]. The calculation of phase content was performed using Rietveld refinement. After indexing the XRD pattern, the lattice constant was calculated using Bragg's law (and Miller indices). The crystalline size of the coatings was calculated using the Scherrer formula $\tau = \frac{0.9 \cdot \lambda}{\beta . \cos \theta}$, where τ is the mean crystalline size, λ is the X-ray wavelength, β is the line broadening at half maximum intensity, and θ is the Bragg angle.

The hardness of the sputtering targets was tested using a microindentation hardness tester (Buehler) equipped with a Vickers-shaped diamond indenter, which allowed us to determine the $HV_{0.2}$ value. In the case of coatings, the hardness and Young's modulus were determined based on the nanoindentation test (NanoTest Vantage system provided by Micro Materials Laboratory Ltd.). A Berkovich-shaped diamond indenter has been used for all nanomechanical investigations. Before the experiment, equipment was calibrated and the indenter's DAF (diamond area function) was determined for each applied load to measure the indenter's exact shape at its top surface [29, 30]. A load from 5 to 20 mN was used on each sample to determine the load-independent region, i.e., to sufficiently develop the plastic zone of the coating and minimise the effect of the substrate (with the maximal depth of indentation not exciding 10% of the coating thickness). To obtain reliable results (the burden with the lowest possible measurement error), indentations at a given load were repeated 10 times inline mode, with a distance of 50 µm from each other. To eliminate creep in the sample, the maximum load was held constantly for 2 s. Each loading and unloading curve was recorded at 10 and 5 s. The hardness and Young's modulus values were calculated on the basis of the Oliver and Pharr method, considering the elastic unloading part of the created load–displacement curve.

The surface roughness of the films was measured with a VK-X100 laser confocal microscope (Keyence, Mechelen, Belgium). The measurements were conducted according to the ISO 4288 standard. Five profiles were tested on each of the surfaces. The arithmetic mean roughness values, Ra, were determined.

3 Results and discussion

3.1 Study on the influence of Ta content on the properties of $W_xTa_{1-x}B_{2-x}$ targets

The ceramic targets were SPS-ed with a 2.5 B: W atomic ratio instead of 2 due to our previous experiments, where

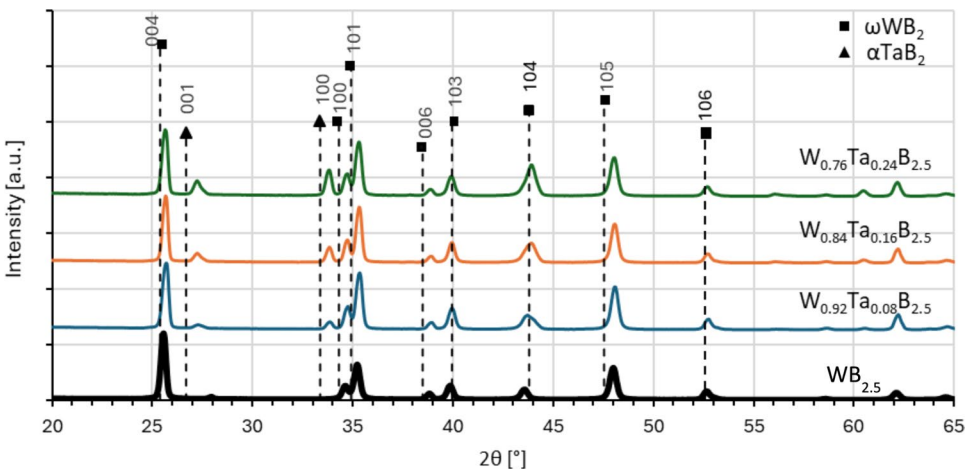

Fig. 2 XRD spectra of $WB_{2\cdot5}$ targets doped with Ta

sputtering a $WB_{2.5}$ target resulted in a coating with boron deficiency [17]. Additionally, such a composition is adequate for the energetically preferred structure WB_2 ($P6_3/mmc$) usually obtained in bulk materials [31]. In Fig. 2, it can be observed that the $WB_{2.5}$ target was composed of the ω-WB_2 ($P6_3/mmc$) phase with lattice parameters a = 2.888 Å and c = 13.920 Å (theoretical lattice parameters a = 2.983 Å, c = 13.879 Å). Doping with 8, 16 and 24% Ta caused the diffraction lines to be shifted towards larger diffraction angles, which means the lattice parameters change to the following: a = 2.881 Å and c = 13.864 Å. The shift of the WB_2 peaks results from obtaining of solid solution through the substitution of tungsten by small amounts of transition metals. Moreover, as a result of a growing amount of Ta, the intensity of the diffraction lines at $2\theta = 27.2°$ and 33.8° (α-TaB_2) increased. Fuger et al. [12] demonstrated that the ω-phase has a lower formation energy than the α-phase except for highly defective structures; however, applied doping does not result in a change to the α-phase. This is due to the sintering of the target materials with excess boron (B/(W + Ta) = 2.5), thereby avoiding the formation of boron point defects, which are beneficial in stabilising the α-phase.

The hardness of the SPS targets increased with Ta concentration, see Fig. 3. The target without Ta doping shows the lowest hardness value of 22.1 ± 1.8 GPa. As a result of increasing tantalum content in the target from 8 to 24%, the hardness increases from 24 ± 2.5 to 25 ± 1.9 GPa.

The XRD spectra and the hardness of $W_{1-x}Ta_xB_{2.5}$ are similar to the results of high-pressure synthesised hexagonal WB_2 presented in the literature [32]. The addition of Ta causes an increase in the lattice constant due to replacing tungsten atoms with tantalum atoms and intrinsic hardening due to solid solution hardening. As it was presented in ref. [11] further increases in tantalum content above 8 at.% can be caused by the appearance of TaB_2 particles and further extrinsic hardening. However, in the case presented in Fig. 3 a growth of hardness with increasing amount of Ta is in the range of measurement error.

3.2 Study of the influence of Ta content on the properties of $W_xTa_{1-x}B_{2-z}$ coatings deposited with RF magnetron sputtering

Coatings were deposited by RF magnetron sputtering from the aforementioned targets with different contents of Ta using parameters described in Sect. 2.1: "Deposition process". Deposited coatings were composed of the α-WB_2 phase. The (0001) peak of α-TaB_2 is also present at ~ 27.5°, see Fig. 4. Sputtering material was deposited on a Si substrate heated to a temperature of 500 °C.

The positions of the diffraction lines also change as they move towards lower diffraction angles. Fuger et al. [12] observed a similar shift, but it should be noted that coatings deposited with the RF method (this work) also contain α-TaB_2-that can cause a shift and broadening of the diffraction peaks In the next step, a change in network constants was designated (Fig. 5). Due to the presence of only single diffraction lines it was impossible to calculate constant a. In the case of the α-WB_2 phase, the c lattice constant was reduced from 3.122 to 3.086 Å. The shortening of the c lattice constant is in agreement with the theoretical calculations presented by Moraes et al. [10]. The introduction of boron vacancies into the supercell causes a significant decrease in lattice parameter c. The presence of boron vacancies in RF-sputtered films is confirmed by the results of composition measurements showing a much lower amount of boron than stoichiometric (B: W = 2) in deposited films (see Fig. 11 in the next section).

In Fig. 6, the influence of tantalum content on the microstructure is presented. Results of SEM investigations clearly

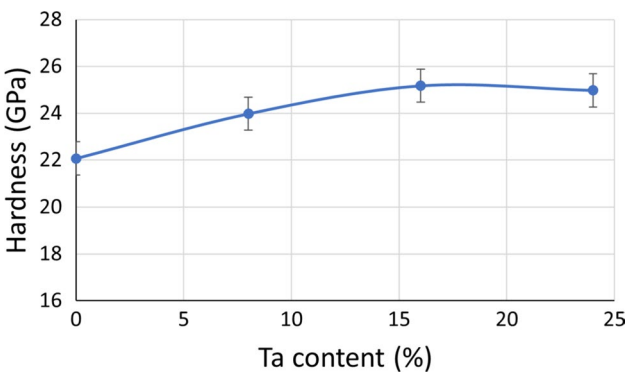

Fig. 3 Microhardness $HV_{0.2}$ as a function of Ta (in at. %) content x in the $W_{1-x}Ta_xB_{2.5}$ targets

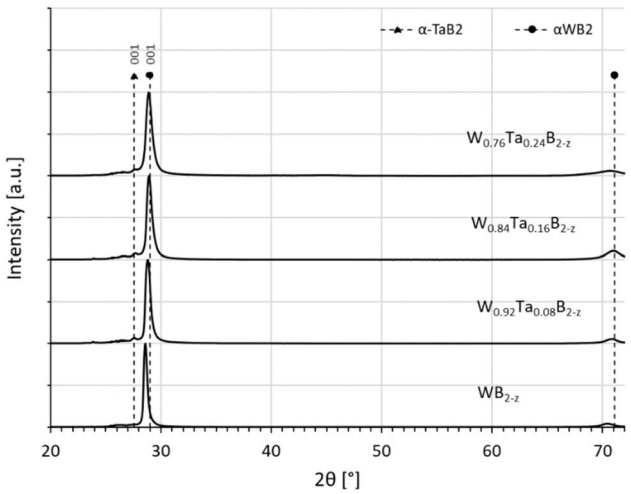

Fig. 4 Diffraction pattern of $W_{1-x}Ta_xB_{2-z}$ coatings doped with Ta and deposited by RF magnetron sputtering at 500 °C

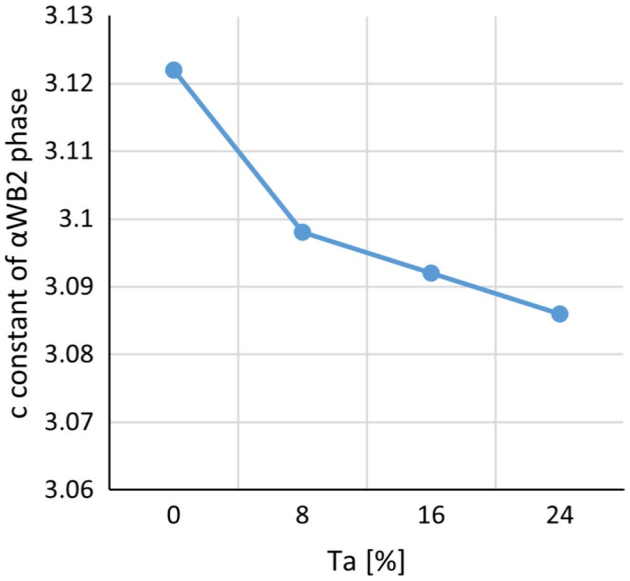

Fig. 5 Lattice constant c of the α-WB_2 phase in coatings doped with Ta (in at. %) and deposited by RF magnetron sputtering at 500 °C

show that the addition of tantalum changes the microstructure of deposited films. The surfaces of coatings without tantalum possess a more fine microstructure than those with 24% tantalum. The fibres are relatively straight, and this is a homogeneous structure along the thickness of the film that is confirmed by the XRD pattern (Fig. 4), where only one peak (0001) of the dominant α-WB_2 phase is present. Due to Barna et al. [33], the crystalline columns grow out of the primary nuclei and proceed to the top of the film; they are often collected into bundles. In the case of coatings with tantalum, the microstructure changes and is less homogeneous along the film thickness. The growth of oriented grains develops the columnar structure; however, the decreased mobility of grain boundaries contaminated with tantalum limits further grain growth. Due to this, such coatings are fine and crystalline at the substrate but can be columnar in the upper part of the films, see Fig. 6d.

The effect of tantalum doping on the hardness of $W_{x-1}Ta_xB_{2-z}$ is presented in Fig. 7. The hardness of the coatings increases with increasing tantalum content, reaching a maximum of 36.9 GPa at a tantalum content of 16%. Further increases in tantalum content did not significantly change the hardness. However, it should be noted that some error bars in Fig. 7 are large, particularly for coatings doped with 8

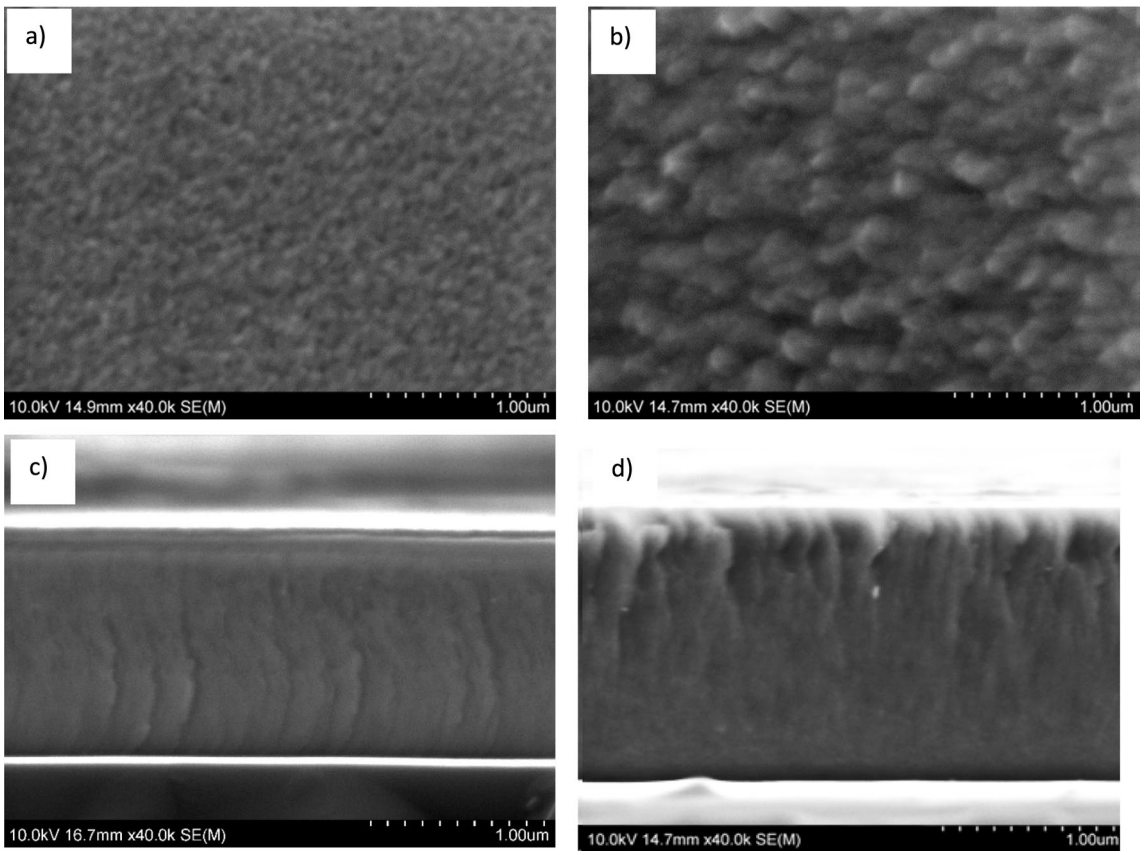

Fig. 6 Surface and cross-sectional SEM images of films without Ta **a**, **c** and RF-deposited from the target with 24% Ta **b**, **d**

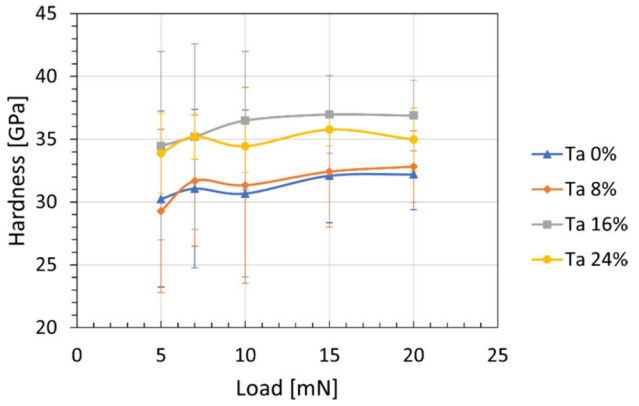

Fig. 7 Nanoindentation hardness of WB_{2-z} doped with Ta (in at. %). Coatings deposited by RF magnetron sputtering at 500 °C

and 16% Ta. In these cases, some of the load–displacement curves were affected by a pop-in effect, indicating a more brittle character. Since the error was defined as the standard deviation of 10 measurements, it can be observed that the error is lower with 24% Ta and results for coatings were more repeatable. The similar increasing trend in hardness with increasing amounts of tantalum can be related to solid solution hardening effects, including parelastic and dielastic contributions such as α-TaB_2 with α-WB_2 having different lattice parameters (Fig. 5b) and shear moduli [31]. Also, the change in microstructure from columnar, perpendicular to substrate to microstructure with grains at different directions can introduce additional strengthening mechanisms [34]. Such a microstructure can be observed, for example, in the case of HiPIMS coatings deposited at a temperature of 400 °C (see Fig. 15), where characteristic "*v*"-shaped grains appear near the substrate.

The effect of tantalum content on the reduced Young's modulus of WB_{2-x} is presented in Fig. 8. It can be observed that doping with 8 and 16% Ta resulted in similarly reduced Young's moduli of 325 and 319 GPa, respectively. Doping with 24% tantalum resulted in a significant decrease in Young's modulus, down to 301 GPa for greater loads, but is similar at 5 mN. The elastic modulus is more sensitive to the effect of substrate. Therefore, the elastic module should be designated for the lower loads. Linear fitting towards 0 loads gives even higher values. For RF-deposited coatings at 500 °C it reaches 380 GPa (please compare with Fig. 21). The lack of dependence of Young's modulus on the amount of tantalum in the range up to $x = 0.24$ is consistent with previous results presented in the literature [12].

3.3 Study of the influence of Ta content on the properties of $W_xTa_{1-x}B_{2-z}$ coatings deposited with HiPIMS

Deposition with HiPIMS sputtering changes the microstructure of deposited films. In the XRD pattern, new reflections from the (0101) and (0002) crystal planes of α-WB_2 are presented (Fig. 9). This can indicate a more inhomogeneous arrangement of grains. The HiPIMS-deposited films have a higher crystallite size compared to the RF-magnetron deposited specimens, indicating that deposition energy plays a vital role in crystallite growth. The highest particle energy with a connection to a lower deposition rate, which is characteristic of the HiPIMS method [25], results in more substantial species bombardment on the growing film. Thanks to this, W-Ta-B crystallites form and grow more rapidly. For example, the crystallite sizes are 77.1 and 62.3 nm for HiPIMS and RF-sputtering, respectively, for films deposited from a 24% Ta target. Similarly to RF-sputtering, a shift of the peaks towards lower angles can be observed as the amount of tantalum increases. HiPIMS-deposited coatings with different content of tantalum are crystalline and possess columnar structure (Fig. 10).

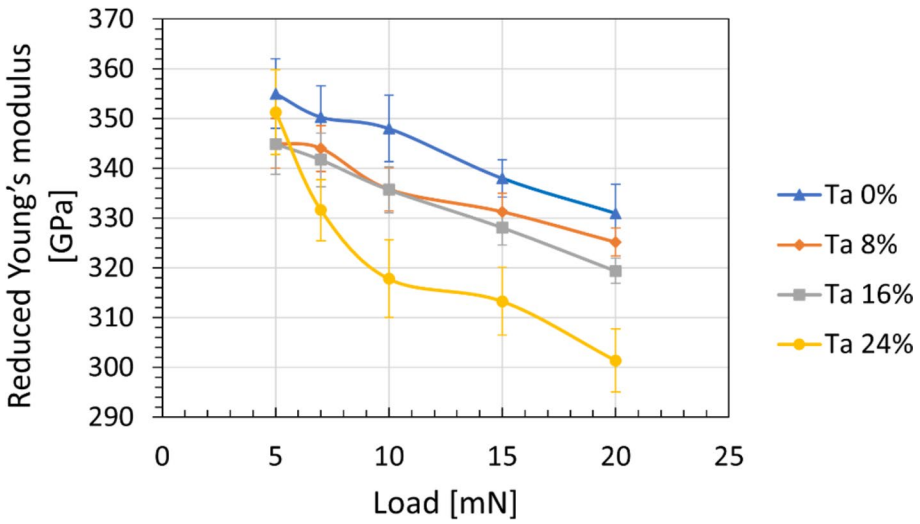

Fig. 8 Reduced Young's moduli of WB_{2-x} doped with Ta (in at. %) and deposited by RF magnetron sputtering at 500 °C

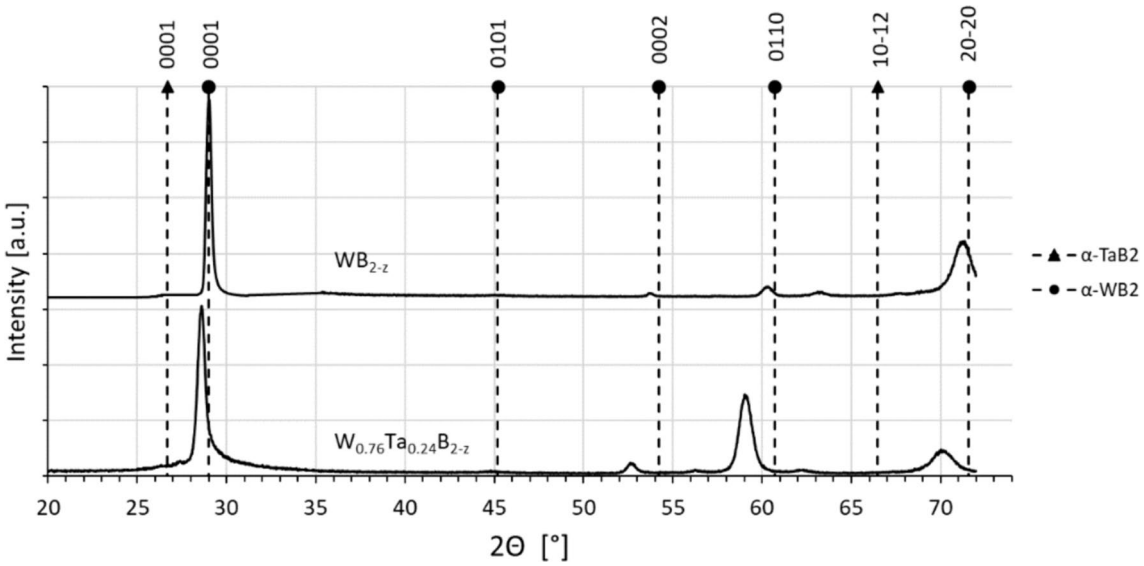

Fig. 9 Diffraction pattern of WB_{2-z} and $W_{1-x}Ta_xB_{2-z}$ coatings deposited by HiPIMS magnetron sputtering at 500 °C

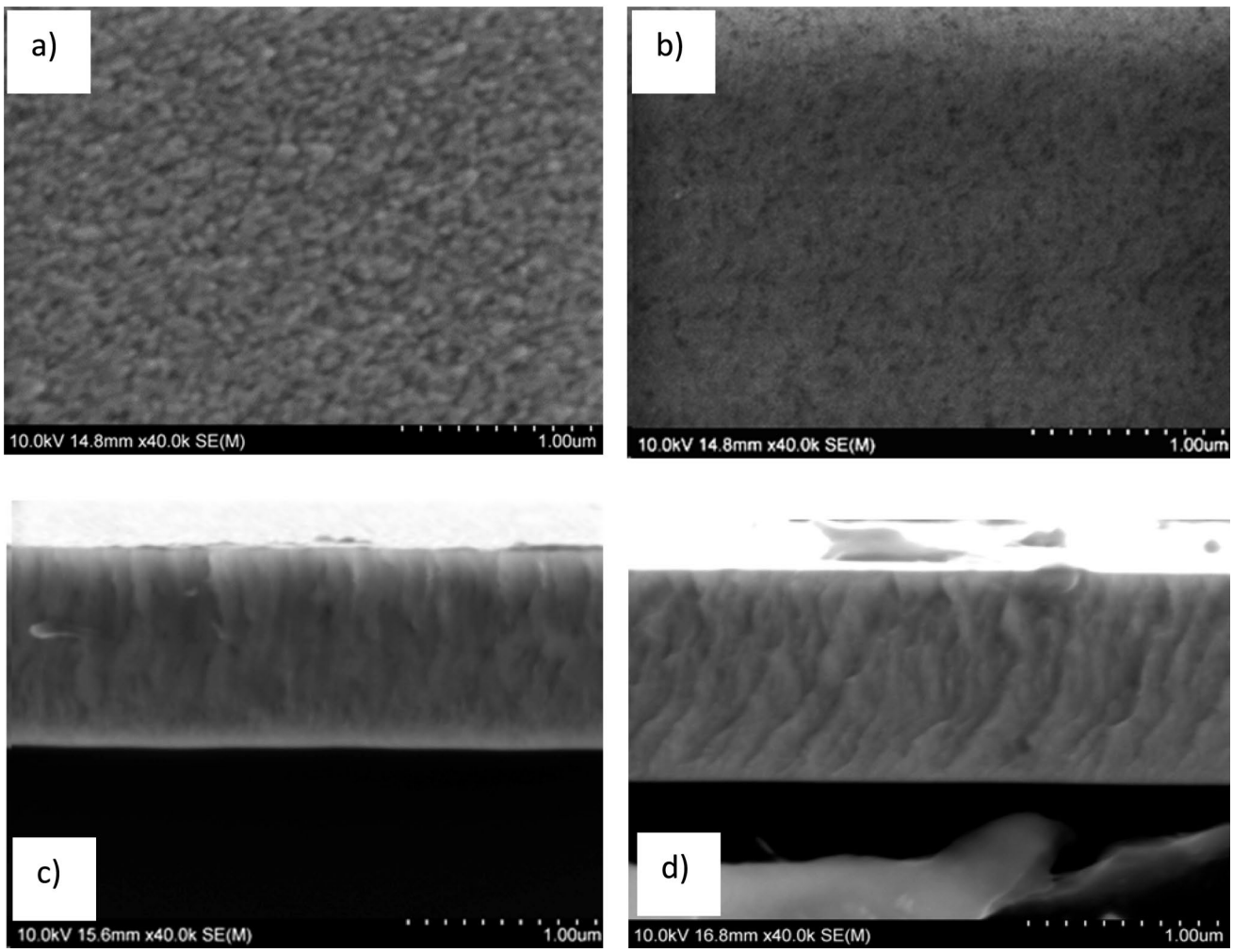

Fig. 10 Surface and cross-sectional SEM images of films without Ta **a**, **c** and HiPIMS-deposited from target with 24% of tantalum **b**, **d**

In opposition to RF-deposited films, the addition of tantalum in HiPIMS coatings causes a less grainy surface (Fig. 10). Additionally, surface feature evolution is determined by lower deposition rates. The thickness of HiPIMS-deposited films is significantly lower than in RF-deposited films, and it is connected with a different ionisation mode during target resputtering and a subsequent decrease in the amount of material reaching the substrate. During HiPIMS sputtering, an increase in surface diffusion means that defects and the porous grain boundaries are filled with deposited material. The films are more dense and their thickness decreases. SEM observations and XRD pattern analysis show that the grain size decreases with increasing Ta content.

Results of composition measurements with EDS show differences in boron and tantalum content in RF- and HiPIMS-deposited coatings (Fig. 11). Regardless of the composition of the sputtering target, the differences in the amount of tantalum in the films compared to the composition of the target are small. It should be noted that, in the case of HiPIMS-sputtering, the amount of tantalum is slightly greater than the stoichiometric composition of the target, while for RF-sputtering there is the opposite relationship. During HiPIMS deposition, the sputtered material is more ionised and can be more easily attracted to the substrate [35]. In the RF method, argon is mainly ionised, and attraction by the substrate can cause additional resputtering of low-mass boron atoms [36]. However, in the case of HiPIMS sputtering, the amount of boron in coatings is much lower than in the RF method. The lowest value is observed in films deposited from a target without Ta and grows when the amount of Ta increase. Overall, a much lower content of boron in deposited coatings for different methods can be related to different angular resputtering of the elements used in the targets, and it is also connected with the dynamics of the plasma. Low-mass boron atoms collide with argon atoms and with the significantly heavier tungsten and tantalum particles, which causes their dispersion. In the case of HiPIMS, a larger amount of heavier and more energetic metal compared to argon ions causes a greater resputtering of light boron in plasma [20].

Boron deficiency has a positive effect on the mechanical properties of coatings. The vacancies stabilise the metastable α-WB_2 phase and, at the same time, the hardness of the coatings increases. The hardness increases with the amount of tantalum from 34.1 ± 1 GPa for 8% Ta to 41.3 ± 3 GPa for 24% Ta (load 10 mN), as shown in Fig. 12. Compared to RF-deposition, the hardness is higher and it results from smaller grains which may hinder the movement of dislocations (Hall Petch effect) and a higher amount of boron vacancies [37].

As hardness increases, the reduced Young's modulus also increases. The reduced Young's modulus, resulting from the linear fitting to low loads, reaches a value of 387 GPa for 24% Ta (Fig. 13). The difference in E^* between both deposition methods is small, and the plasticity index (H/E^*) is higher for HiPIMS-sputtering. For example, H/E^* is 0.088 for 8% Ta and 0.107 for 24% Ta, while for RF-sputtering it is 0.081 for 0% Ta and 0.096 for 16% Ta. An increase in the plasticity index indicates an increase in the ductility of the deposited films.

Considering that doping WB_{2-z} with 24% tantalum causes the highest increase in the hardness without significant

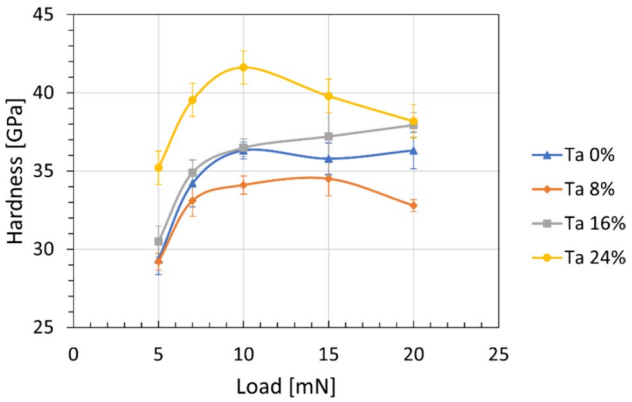

Fig. 12 Nanoindentation hardness of WB_{2-x} doped with Ta (in at. %). Coatings deposited by HiPIMS magnetron sputtering at 500 °C

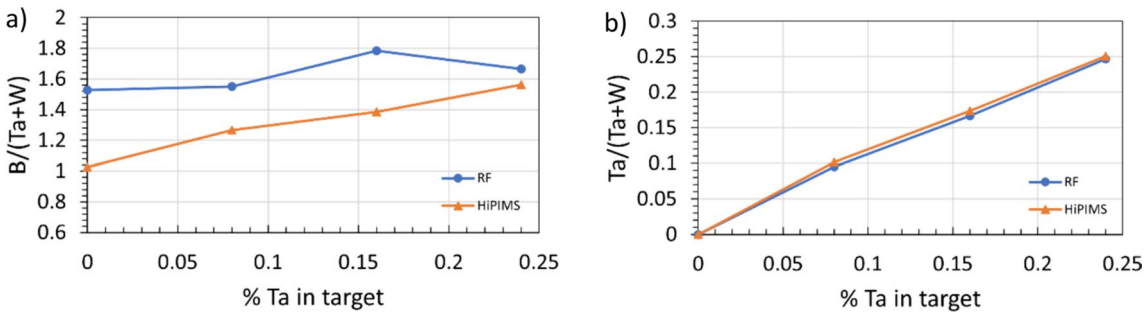

Fig. 11 Composition of RF and HiPIMS coatings: **a** B/(W + Ta), **b** Ta/(W + Ta) ratio. $T_s = 500$ °C (elements content are given in at. %)

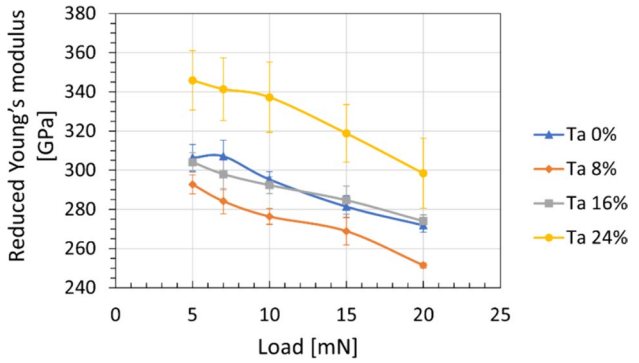

Fig. 13 Reduced Young's moduli of WB_{2-x} doped with Ta (in at. %) and deposited by RF magnetron sputtering at 500 °C

growth of the reduced Young's modulus, it was decided that such coatings would be further used for investigations on the influence of deposition temperature on the properties of the obtained coatings.

3.4 Study of the influence of the substrate temperature on the properties of $W_{0.76}Ta_{0.24}B_{2-z}$ coatings

In the next step, the substrate temperature's influence on the 24% Ta coatings' properties were analysed. The substrate temperature range was 300–600 °C for RF and 200–500 °C for HiPIMS deposition. The difference in the deposition temperature ranges is due to obtaining crystalline microstructures for both methods. The coatings deposited at room temperature peeled off and were measured only by XRD. The roughness and thickness of the coatings deposited at the elevated substrate temperatures were summarised in Table 1.

The data presented in Table 1 indicates that the deposition rate slightly decreases with increasing substrate temperature. According to the structural zone diagram [33], structures deposited at the temperature interval $0 < T_s/T_m < 0.2$ (T_m—melting temperature), where neither the bulk diffusion nor the self-surface diffusion has a remarkable value, are built with crystals that probably contain a high density of defects and porous grain boundaries. The increase of T_s can cause the ordering of the crystals and the decrease in porosity which results in a reduction in the thickness of the films [33].

The microscopic observations in lower resolution show that all deposited coatings have a metallic luster and a similar surface appearance regardless of whether RF and HiPIMS deposition modes were used. An exemplary SEM image of the coatings deposited at 500 °C and the roughness profile measured for both methods are presented in Fig. 14.

In the case of HiPIMS, the deposition rate is much lower than RF (Table 1). This can be explained by the fact that the pulse's short duration increases the pulse's energy density and thus increases the number of metal ions sputtered from the target [38]. These ionised elements undergo back-attraction to the target and, therefore, do not reach the substrate. In the case of RF [21] and HiPIMS [20], ion energies range amounts to 0–50 eV. The difference between both methods is that, in the case of RF, Ar^+ ions dominate, while for HiPIMS their intensity decreases by at least an order of magnitude and the number of ions of the sputtered material increases significantly. Energetic high-intensity fluxes of metal ions reaching the substrate cause differences in the growth of layers. Applying ion-assisted deposition (HiPIMS) can enhance adatom mobility and facilitates atoms to move about on the surface and fill some of voids which allows the material to obtain a denser microstructure.

The surface of the coatings deposited on the heated Si substrate is smooth (Table 1). Several droplets per 100×100 µm have been spotted, see Fig. 14. In both RF and HiPIMS sputtering, droplets were up to 800 nm in diameter and below 100 nm in height. In the case of HiPIMS sputtering, one of the causes of debris deposition is the arcing phenomenon [39]. Arcing means the

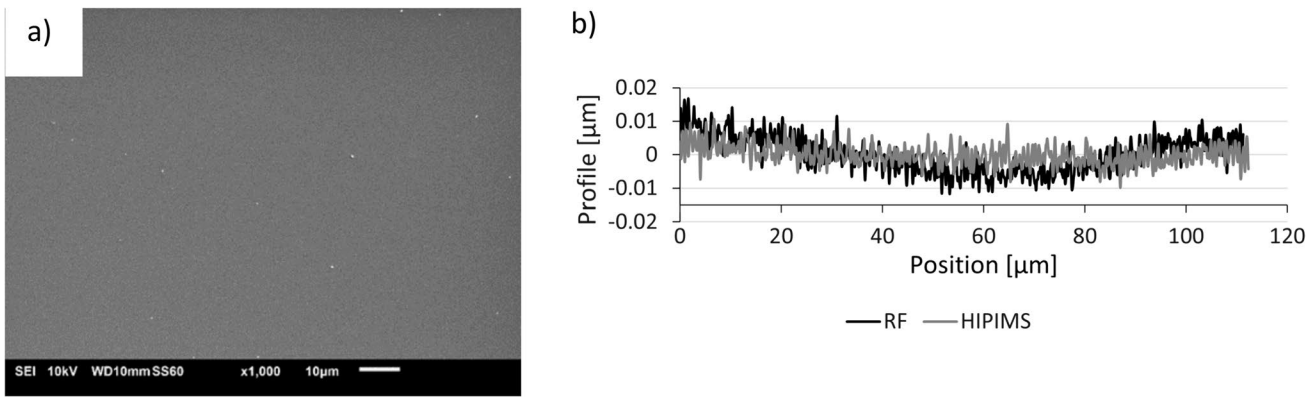

Fig. 14 SEM image of the exemplary coatings deposited at 500 °C **a** and the roughness profile of coatings deposited at 500 °C **b**

appearance of cathodic arc discharges with small cathode spots on the target. Discharge arcing leads to the ejection of microscopic target debris which will lead to the deposition of undesirable droplets and cause defects in the coatings. In the case of using SPS-ed targets, the problem is more serious due to the porosity and non-uniformity of the disc [40]. The quality of the target is much less important when using RF sputtering. In this case, due to the different types of modes of excitation, arcs on the target surface practically do not occur.

The surfaces of the coatings (without taking into account the droplets) are characterised by a low R_a roughness value of a few nm, see Table 1. At lower deposition temperatures, the HiPIMS coatings show more smooth surfaces (Fig. 15), unlike the RF method (Fig. 16). This is a result of a different mechanism of microstructure growth.

In agreement with the structural zone diagram [33], coatings deposited with lower particle energy (RF) and the temperature interval $0.1 < T_s/T_m < 0.4$ are usually deposited in Zone I. Such coatings are characterised by a homogeneous structure with thin columnar grains along the film thickness (Fig. 16). Increasing the deposition temperature does not cause a change in this property. However, the crystallisation of RF-deposited films starts at a surface temperature above 400 °C. In the case of HiPIMS coatings, where arriving substrate particles possess higher energy, the structure becomes inhomogeneous and is defined as ZONE T. SEM observations (Fig. 15) and XRD analysis

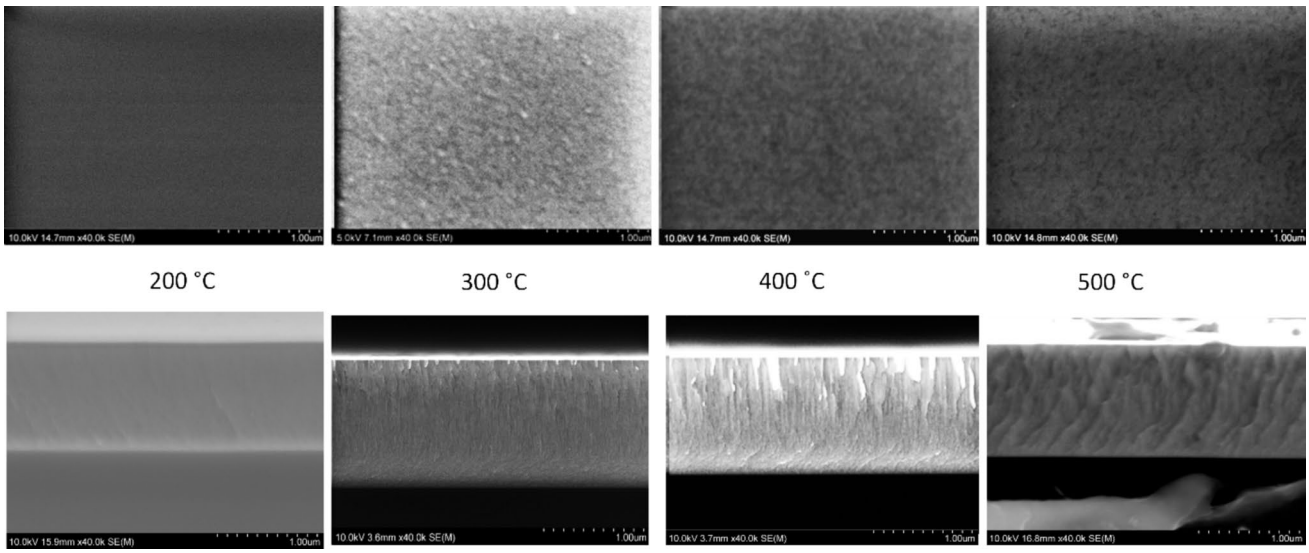

Fig. 15 Surface and cross-sectional SEM images of HiPIMS-deposited films at elevated substrate temperatures

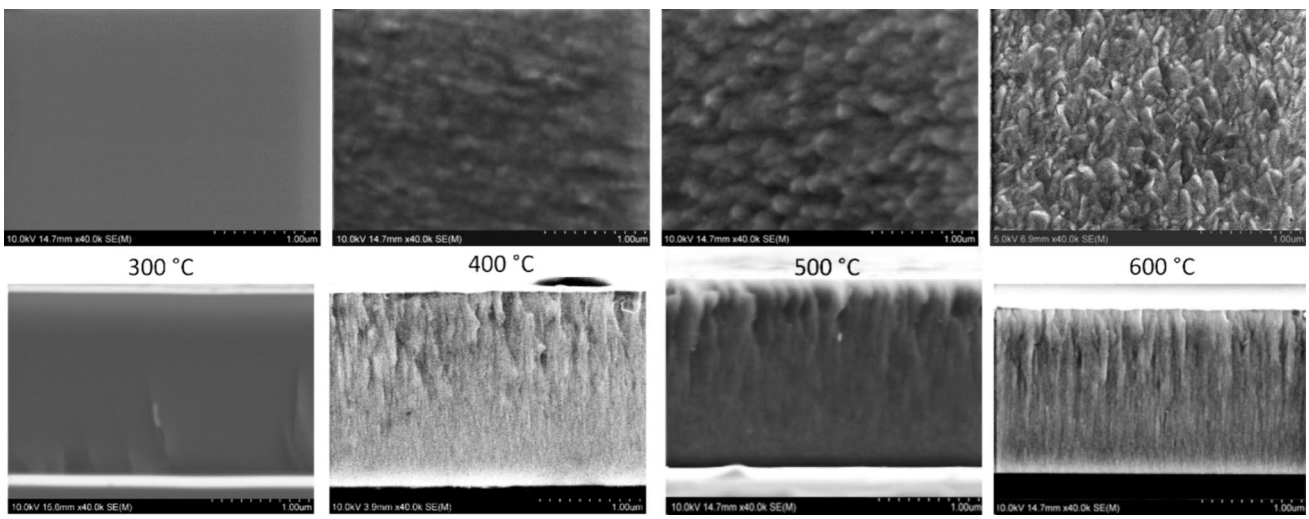

Fig. 16 Surface and cross-sectional SEM images of RF-deposited films at elevated substrate temperatures

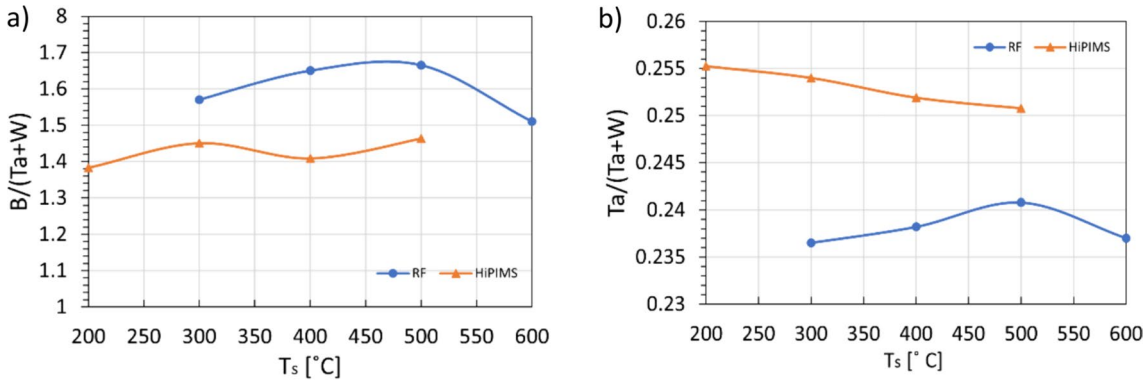

Fig. 17 EDS results: **a** B/(W + Ta) ratio, **b** Ta/(W + Ta) ratio in RF- and HiPIMS-deposited films at different substrate temperatures

show that crystalline coatings are obtained for this method at a lower substrate temperature of 300 °C. In the case of RF, the increase in temperature results in smoother surfaces due to greater adatom surface mobility.

The EDS analyses of the $W_{0.76}Ta_{0.24}B_{2-x}$ coatings were focused on comparing the B/(W + Ta) and Ta/(W + Ta) ratios. The results of the compositions obtained for both methods at elevated temperatures are presented in Fig. 17.

In the case of RF-deposited coatings, the B/(W + Ta) ratio is from 1.51 to 1.66 and the Ta/(W + Ta) ratio is from 0.237 to 0.240. Considering the measurement's accuracy [41], both are independent of temperature. In the case of HiPIMS coatings, the B/(W + Ta) ratio is from 1.39 to 1.44. The Ta/(W + Ta) ratio decreases with temperature from 0.254 to 0.251. The RF coatings have about 8–12% higher boron content and 4–7% lower Ta content than HiPIMS coatings at the same substrate temperature. During HiPIMS deposition, the plasma reaching the substrate is composed primarily of high-energy ionised substrate material. The impact of high-energetic particles can cause preferential resputtering of the film-forming adatoms [20, 42]. The energies of the atoms reaching the substrate during RF deposition are much lower, so fewer boron atoms are knocked out. Sroba et al. [36] also showed that the substoichiometric composition in the case of TaB_2-x may be influenced by reflected neutral Ar. Influencing the kinetic energy of Ar neutrals that cause resputtering of light boron from the growing films via the target voltage (above 400 V) leads to the formation of substoichiometric TaB_2-x films, for example.

The phase composition and crystallite size analysis were performed based on XRD spectra presented in Figs. 18 and 19.

The XRD analysis confirms the earlier SEM observation of the specimens' surfaces and cross-sections that RF-deposited coatings below 300 °C are amorphous. Increasing the temperature of the substrate favours the formation of fine-grained α-WB_2. However, at temperatures below 600 °C,

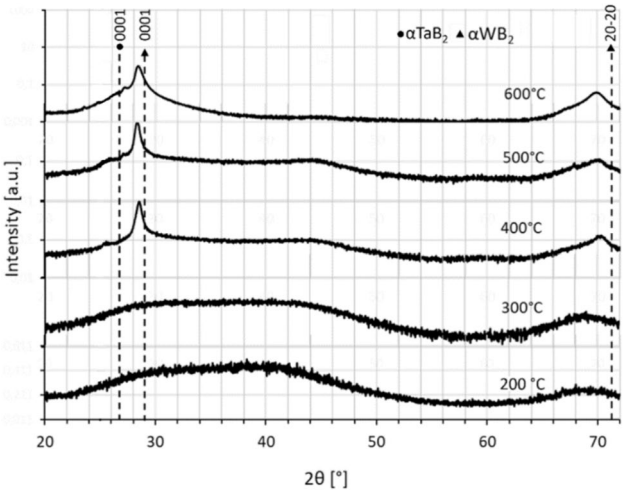

Fig. 18 XRD spectra of $W_{0.76}Ta_{0.24}B_{2-z}$ coatings deposited on substrates of different temperatures. Type of power supply–RF. The scaling of the y-axis is logarithmic

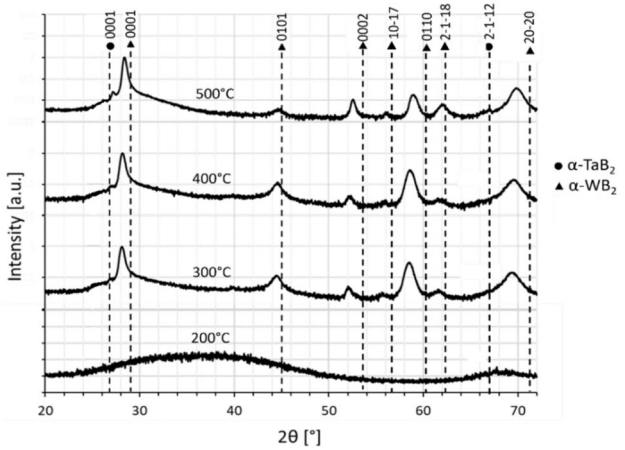

Fig. 19 XRD spectra of $W_{0.76}Ta_{0.24}B_{2-z}$ coatings deposited on substrates of different temperatures. Type of power supply–HiPIMS. The scaling of the y-axis is logarithmic

Table 2 Summary of XRD analysis results for RF and HiPIMS coatings

Substrate temp. (°C)	RF		HiPIMS	
	Crystallite size (nm)	The lattice parameters	Crystallite size (nm)	The lattice parameters
300	Amorphous		α-WB_2: 53.4	α-WB_2: a = 3.044 Å, c = 3.17 Å
400	α-WB_2: 87.0	α-WB_2: c = 3.126 Å;	α-WB_2: 57.5	α-WB_2: a = 3.051 Å, c = 3.16 Å
500	α-WB_2: 88.0	α-WB_2: c = 3.138 Å;	α-WB_2: 77.1	α-WB_2: a = 3.054 Å, c = 3.144 Å;
600	α-WB_2: 88.9	α-WB_2: c = 3.142 Å;		

a broad diffraction line at 2θ between 24° and 48° was observed, indicating the presence of an amorphous phase.

The presence of single diffraction lines indicates the preferred direction of growth: (0001) for the α-WB_2 phase. Due to the presence of only single diffraction lines, only the lattice constant c was calculated. In Table 2, it is visible that the c constant lattice of the α-WB_2 phase increases from 3.126 to 3.142 Å with a temperature increase from 400 to 600 °C. An increase in lattice constants can be connected with a rise in compressing stress due to significant concentrations of trapped gas atoms. Such a dependence is characteristic of RF deposition, where the surface of the substrate is mainly bombarded by gas-ions (e.g., Ar^+) during the growth of films due to low levels of sputter-material atom ionisation, ≤ 1% [43].

The HiPIMS coatings are crystalline from 300 °C; therefore, at a lower temperature than RF coatings. As in the case of RF coatings, HiPIMS coatings are mainly composed of a fine-grained α-WB_2 phase with a preferred (0001) orientation. However, exact analysis of the XRD pattern (the logarithmic scaling of the *y*-axis) also shows other orientations, which are connected with the inhomogeneous microstructure presented in Fig. 15. The broadening of the XRD peaks with increasing Ta content is minimal, suggesting that the coherently diffracting domain sizes and microstrains are comparable for all coatings [13]. The lattice constant c of the α-WB_2 phase decreases from 3.17 to 3.144 Å with the temperature increasing from 300 to 500 °C. An overview of the XRD analysis is presented in Table 2. Such levering of lattice constants is connected with a change of the position of the peaks towards higher angles, which is caused either by stress relaxation of the coating or by structural changes in the coating with an increase in temperature. Stress relaxation of the coatings includes different stress- and strain-driven phenomena such as adatom migration and the movement of defects, grouping of point defects, reorganisation and annihilation of dislocations, growth, and coalescence of sub-grains or plastic flow [44].

The α-WB_2 phase lattice constants shown increased compared to the theoretical ones (the theoretical lattice parameters of α-WB_2 are a = 3.02 Å and c = 3.05 Å). The increase in the lattice constants a and c for the α-WB_2 phase compared to the constants of the undoped α-WB_2 has already been noticed by Moraes et al. [10]. This effect is attributed to the presence of tantalum doping (theoretical lattice parameters of α-TaB_2 are a = 3.098 Å and c = 3.227 Å). In the case of HiPIMS-deposited coatings, the decrease in the lattice constant c with increasing deposition temperature can be explained by a slight decrease in tantalum content.

Nanoindentation hardness of the deposited coatings is presented in Fig. 20 and the reduced Young's modulus is

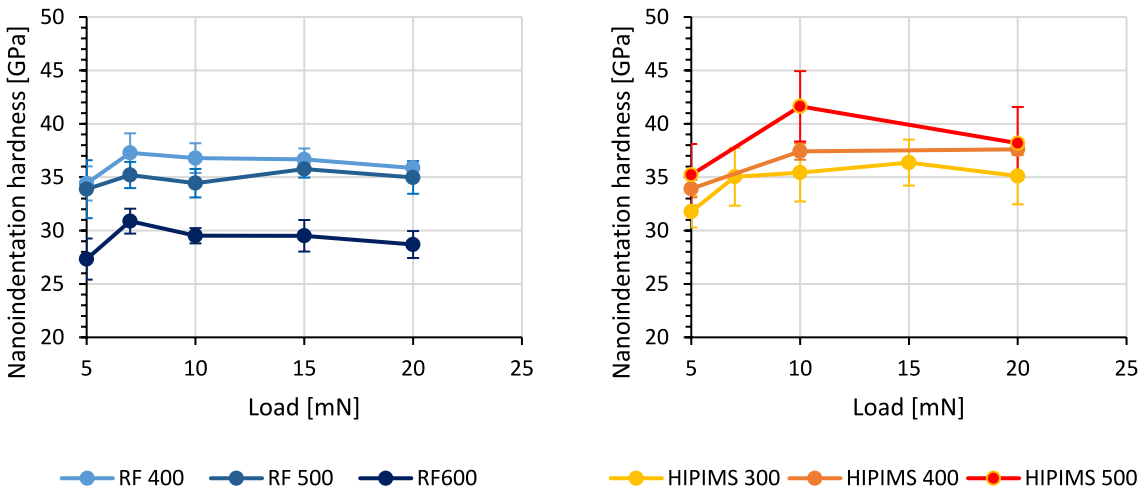

Fig. 20 Nanoindentation hardness of the coatings deposited with RF power supply (left) and HiPIMS power supply (right)

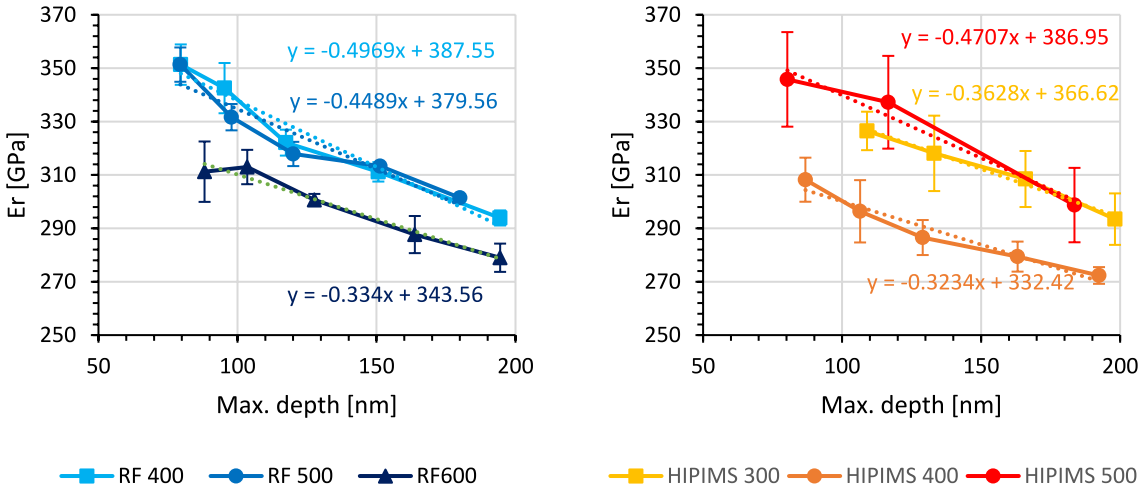

Fig. 21 Reduced Young's modulus of the coatings deposited with RF power supply (left) and HiPIMS power supply (right)

shown in Fig. 21. RF-deposited coatings at a substrate temperature of 400 and 500 °C have a hardness of 35.5 ± 0.5 GPa. An increase of the substrate temperature to 600 °C resulted in a decrease in hardness to 28.7 ± 0.3 GPa, which is connected with the increase of α-TaB_2 phase content and disruption of the crystal structure and phase separation. Another explanation is that hardness decreases at $T_s > 500$ °C due mainly to column coarsening and planar defect annihilation [34]. In the case of HiPIMS coatings, hardness remains constant at about 36.5 GPa regardless of temperature. Higher values of hardness for HiPIMS-deposited coatings are primarily attributed to a different microstructure and the lower grains (Hall–Petch effect [34]).

The reduced Young's modulus of RF coatings decreases from 387 to 343 GPa (approximation to 0 load, Fig. 21) as the temperature increases from 400 to 600 °C. In the case of HiPIMS-deposited coatings, the trend is similar and the reduced Young's modulus decreases from 387 to 332 GPa, which has a positive effect on reducing the brittleness of the material.

4 Summary

This research focused on the study of HiPIMS and RF magnetron sputtered W-Ta-B_{2-z} thin-film coatings from one SPSed target.

The first part of the paper presents the effect of tantalum doping on the hardness and phase composition of RF- and HiPIMS-deposited ceramic coatings. It has been observed that an increase in the tantalum content from 8 to 24% allows for maintaining a high hardness of 35 GPa for RF-sputtering and 41.3 GP for HiPIMS-sputtering. Comparing HiPIMS deposition to RF deposition, the hardness is higher and it results from the rebuilding of the crystal structure from columnar to a heterogeneous-like zone T microstructure with smaller grains. At the same time, the value of the reduced Young's modulus is about 380 GPa for both methods which means that the plasticity index (*H/E**) is higher for HiPIMS-sputtering. For HiPIMS-deposited coatings at 500 °C, *H/E** is 0.107 (24% Ta), while for RF-sputtering it is 0.096. An increase in the plasticity index indicates an increase in the ductility of the deposited films.

In the second part of the paper, the coatings deposited with RF and HiPIMS with substrate temperatures from 200 to 600 °C were compared. The hardness of RF-deposited films decreases with an increase in temperature, from 28.7 GPa to 35 GPa, while increasing from 36.5 to 41.3 GPa for HiPIMS-deposited films. The thickness of HiPIMS-deposited films is relatively small: only around 60% of the RF magnetron sputtered coatings, even when the average power input was two times higher. The deposition rate reduction effect is usually attributed to the fact that some of the newly formed sputtering ions return to the target. On the other hand, it has been shown that the RF coatings require heating the substrate above 400 °C to obtain a fully crystalline structure, and HiPIMS-deposited coatings allow for a reduction of the substrate temperature to 300 °C. Both coatings possess surfaces with smooth morphologies, but the HiPIMS method requires better quality targets to limit arcing on the surface.

By controlling the deposition parameters, RF magnetron sputtering and HiPIMS are effective methods for the deposition of W-Ta-B coatings with suitable morphologies and hardness, making them more appropriate for industrial applications as surface protective coatings. Films deposited by the HiPIMS method have a higher plasticity index, which means that they are more resistant to cracking and therefore more reliable. In the case of the HiPIMS method, however, the problem is the low deposition rate for short

pulses. This can be solved by increasing the pulse length for example. Due to the use of one magnetron, which also influences the deposition rate, the method presented in this article is simplified. Additionally, lowering the temperature during deposition is beneficial for temperature-sensitive substrates, covering large elements whose dimensions make uniform heating impossible. In the case of HiPIMS, the relatively low deposition rate is one of the main challenges in terms of the economic efficiency of the deposition process.

Taking into account the application approach, the key parameter is to reduce the deposition temperature while maintaining or improving mechanical properties. Based on the analysed cases, the best results were obtained when coatings were deposited with a concentration of 24% at. tantalum at 400 °C. Despite the temperature reduction, the H/E* ratio is the highest (0.123) and at the same time the layers are slightly below the super hardness limit (38 ± 1 GPa). High hardness combined with reduced brittleness of the material should have a positive effect on the wear resistance of coatings applied, for example, on forging or extrusion tools, where the dies may have a large mass and achieving high temperature on the deposited surface is very difficult.

Acknowledgements The Authors E. W. and L. K. were supported by the European Union Horizon 2020 research and innovation program under Grant Agreement No. 857470 and from the European Regional Development Fund under the program of the Foundation for Polish Science International Research Agenda PLUS, grant No. MAB PLUS/2018/8, and the initiative of the Ministry of Science and Higher Education 'Support for the activities of Centers of Excellence established in Poland under the Horizon 2020 program'; under agreement No. MEiN/2023/DIR/3795.

Funding This work was funded by the National Centre for Research and Development (NCBR, Poland) under project no. TECHMATSTRATEGIII/0017/2019—purchase of a coatings deposition system and synthesis of targets) and National Science Centre (NCN, Poland) 2022/47/B/ST8/01296—other research.

Data availability Data sets generated during the current study are available from the corresponding authors on reasonable request.

Declarations

Conflict of interest The authors declare no conflict of interest.

References

1. Magnuson M, Hultman L, Hogberg H. Review of transition-metal diboride thin films. Vacuum. 2022;196:110567.
2. Fiantok T, Koutná N, Sangiovanni D, Mikula M. Ceramic transition metal diboride superlattices with improved ductility and fracture toughness screened by ab initio calculations. Sci Reports. 2023;13:12835.
3. Akopov G, Yeung MT, Kaner RB. Rediscovering the crystal chemistry of borides. Adv Mater. 2017;29:1604506.
4. Chrzanowska J, Hoffman J, Denis P, Giżyński M, Mościcki T. The effect of process parameters on rhenium diboride films deposited by PLD. Surface Coat Technol. 2015;277:15–22.
5. Mościcki T, Psiuk R, Jarząbek D, Ciemiorek-Bartkowska M, Kulikowski K, Jasiński J, Włoczewski M, Lewandowska M. Effect of titanium and deposition parameters on microstructure and mechanical properties of W-Ti-B thin films deposited by high power impulse magnetron sputtering. Surface Coat Technol. 2024;485:130915.
6. Maździarz M, Psiuk R, Krawczyńska A, Lewandowska M, Mościcki T. Effect of zirconium doping on the mechanical properties of W1−xZrxB2 on the basis of first-principles calculations and magnetron sputtered films. Arch Civ Mech Eng. 2022;22(193):1–30.
7. Akopov G, Yeung M, Turner C, Mohammadi R, Kaner R. Extrinsic hardening of superhard tungsten tetraborides alloys with group 4 transition metals. J Am Chem Soc. 2016;138:5714–21.
8. Mohammadi R, Turner CL, Xie M, Yeung MT, Lech AT, Tolbert SH, Kaner RB. Enhancing the hardness of superhard transition-metal borides: molybdenum-doped tungsten tetraboride. Chem Mater. 2016;28(2):632–7.
9. Wu Z, Long Y, Lin H-T, Zhang F. Effect of tantalum on phase transition and thermal stability of metastable tungsten tetraboride. Cer Intern. 2020;46:17217–23.
10. Moraes V, Fuger C, Paneta V, Primetzhofer D, Polcik P, Bolvardi H, Arndt M, Riedl H, Mayrhofer P. Substoichiometry and tantalum dependent thermal stability of α-structuredW-Ta-B thin films. Scripta Mater. 2018;155:5–10.
11. Pangilinan L, Turner C, Akopov G, Anderson M, Mohammadi R, Kaner R. Superhard tungsten diboride-based solid solutions. Inorg Chem. 2018;57(24):15305–13.
12. Fuger C, Moraes V, Hahn R, Bolvardi H, Polcik P, Riedl H, Mayrhofer P. Influence of Tantalum on phase stability and mechanical properties of WB2. MRS Commun. 2019;9(1):375–80.
13. Seidl W, Bartosik M, Kolozsvari S, Bolvardi H, Mayrhofer P. Influence of Ta on the fracture toughness of arc evaporated Ti-Al-N. Vacuum. 2018;150:24–8.
14. Musil J. Flexible hard nanocomposite coatings. RSC Adv. 2015;5:60482.
15. Fuger C, Schwartz B, Wojcik T, Moraes V, Weiss M, Limbeck A, Macauley C, Hunold O, Polcik P, Primetzhofer D, Felfer P, Mayrhofer P, Riedl H. Influence of Ta on the oxidation resistance of WB2−z coatings. J Alloys Compd. 2021;864:158121.
16. Mościcki T, Chrzanowska-Giżyńska J, Psiuk R, Denis P, Mulewska K, Kurpaska Ł, Chmielewski M, Wiśniewska M, Garbiec D. Thermal and mechanical properties of (W, Zr)B2-z coatings deposited by RF magnetron sputtering method. Int J Refract Met Hard Mater. 2022;105:105811.
17. Psiuk R, Mościcki T, Chrzanowska-Giżyńska J, Kurpaska Ł, Radziejewska J, Denis P, Garbiec D, Chmielewski M. Mechanical and thermal properties of W-Ta-B coatings deposited by high-power impulse magnetron sputtering (HiPIMS). Materials. 2023;16(2):664.
18. Vega-Morón R, Rodríguez Castro G, Melo-Máximo D, Méndez-Méndez J, Melo-Máximo L, Oseguera-Peña J, Meneses-Amador

A. Adhesion and mechanical properties of Ti films deposited by DC magnetron sputtering. Surf Coat Technol. 2018;349:1137–47.
19. Greczynski G, Lu J, Jensen J, Petrov I, Greene J, Bolz S, Kölker W, Schiffers C, Lemmer O, Hultman L. Metal versus rare-gas ion irradiation during Ti1−xAlxN film growth by hybrid high power pulsed magnetron/dc magnetron co-sputtering using synchronized pulsed substrate bias. J Vac Sci Technol A. 2012;30:061504.
20. Greczynski G, Petrov I, Greene J, Hultman L. Paradigm shift in thin-film growth by magnetron sputtering: From gas-ion to metal-ion irradiation of the growing film. J Vac Sci Technol A. 2019;37:060801.
21. Ellmer K, Cebulla R, Wendt R. Characterization of a magnetron sputtering discharge with simultaneous RF- and DC-excitation of plasma for the deposition of transparent and conductive ZnO:Al-films. Surrf Coat Tech. 1998;98:1251–6.
22. Chrzanowska J, Kurpaska Ł, Giżyński M, Hoffman J, Szymański Z, Mościcki T. Fabrication and characterization of superhard tungsten boride layers deposited by radio frequency magnetron sputtering. Cer Intern. 2016;42:12221–30.
23. Sobol O, Dub S, Pogrebnjak A, Mygushchenko R, Postelnyk A, Zvyagolsky A, Tolmachova G. The effect of low titanium content on the phase composition, structure, and mechanical properties of magnetron sputtered WB2-TiB2 films. Thin Solid Films. 2018;662:137–44.
24. Euchner H, Mayrhofer P, Riedl H, Klimashin F, Limbeck A, Polcik P, Kolozsvari S. Solid solution hardening of vacancy stabilized TixW1-xB2. Acta Mater. 2015;101:55–61.
25. Anders A. A review comparing cathodic arcs and high power impulse magnetron sputtering (HiPIMS). Surf Coat Technol. 2014;257:308–25.
26. Greczyński G, Lu J, Bolz S, Kölker W, Schiffers C, Lemmer O, Petrov I, Greene J, Hultman L. Novel strategy for low-temperature, high-rate growth of dense, hard, and stress-free refractory ceramic thin films. J Vac Sci Technol A. 2014;32:041515.
27. Mościcki T, Psiuk R, Radziejewska J, Wiśniewska M, Garbiec D. Properties of spark plasma sintered compacts and magnetron sputtered coatings made from Cr, Mo, Re and Zr alloyed tungsten diboride. Coatings. 2021;11:1378.
28. Kipkirui N, Lin T-T, Kiplangat R, Lee J-W, Chen S-H. HiPIMS and RF magnetron sputtered Al0.5CoCrFeNi2Ti0.5 HEA thin-film coatings: synthesis and characterization. Surf Coat Technol. 2022;449:128988.
29. McElhaney K, Vlassak J, Nix W. Determination of indenter tip geometry and indentation contact area for depth-sensing indentation experiments. J Mater Res. 1998;13(5):1300–6.
30. Chicot D, Yetna N'Jock M, Puchi-Cabrera ES, Iost A, Staia M, Louis G, Bouscarrat G, Aumaitre R. A contact area function for Berkovich nanoindentation: application to hardness determination of a TiHfCN thin film. Thin Solid Films 2014;558: 259–266. hal-01066329
31. Moraes V, Riedl H, Fuger C, Polcik P, Bolvardi H, Holec D, Mayrhofer PH. Ab initio inspired design of ternary boride thin films. Sci Reports. 2018;8:9288.
32. Yin S, He D, Hu C, Wang W, Wang H, Li L, Zhang L, Liu F, Liu P, Wang Z, Meng C, Zhu W. Hardness and elastic moduli of high pressure synthesized MoB2 and WB2 compacts. High Press Res. 2013;33(2):409–17.
33. Barna P, Adamik M. Fundamental structure forming phenomena of polycrystalline films and the structure zone models. Thin Solid Films. 1998;317:27–33.
34. Bakhit B, Palisaitis J, Wu Z, Sortica M, Primetzhofer D, Persson PO, Rosen J, Hultman L, Petrov I, Greene J, Greczynski G. Age hardening in superhard ZrB2-rich Zr1-xTaxBy thin films. Scr Mater. 2021;191:120–5.
35. Wicher B, Pshyk O, Li X, Bakhit B, Rogoz V, Petrov I, Hultman L, Greczynski G. Superhard oxidation-resistant Ti1-xAlxBy thin films grown by hybrid HiPIMS/DCMS co-sputtering diboride targets without external substrate heating. Mat Des. 2024;238:112727.
36. Šroba V, Fiantok T, Truchlý M, Roch T, Zahoran M, Grančič B, Nagy P, Izai V, Kúš P, Mikula M. Structure evolution and mechanical properties of hard tantalum diboride films. J Vac Sci Technol A. 2020;38:033408.
37. Fuger C, Hahn R, Zauner L, Wojcik T, Weiss M, Limbeck A, Hunold O, Polcik P, Riedl H. Anisotropic super-hardness of hexagonal WB2±z thin films. Mater Res Lett Tom. 2022;10(2):70–7.
38. Gudmundsson J. Physics and technology of magnetron discharges. Plasma Sources Sci Technol. 2020;29: 113001.
39. Anders A. Tutorial: reactive high power impulse magnetron sputtering (R-HiPIMS). J Appl Phys. 2017;121: 171101.
40. Garbiec D, Wiśniewska M, Psiuk R, Denis P, Levintant-Zayonts N, Leshchynsky V, Rubach R. Zirconium alloyed tungsten borides synthesized by spark plasma sintering. Arch Civ Mech Eng. 2021;21:37.
41. Bakhit B, Primetzhofer D, Pitthan E, Sortica M, Ntemou E, Rosen J, Hultman L, Petrov I, Greczynski G. Systematic compositional analysis of sputterdeposited boron-containing thin films. J Vac Sci Technol A. 2021;39:063408.
42. Neidhardt J, Mráz S, Schneider J, Strub E, Bohne W, Liedke B, Möller W, Mitterer C. Experiment and simulation of the compositional evolution of Ti–B thin films deposited by sputtering of a compound targe. J Appl Phys. 2008;104:063304.
43. Li X, Bakhit B, Johansson Jõesaar M, Hultman L, Petrov I, Greczynski G. Toward energy-efficient physical vapor deposition: routes for replacing substrate heating during magnetron sputter deposition by employing metal ion irradiation. Surf Coat Technol. 2021;415:127120.
44. Polaček M, Souček P, Alishahi M, Koutná N, Klein P, Zábranský L, Czigány Z, Balázsi K, Vašina P. Synthesis and characterization of Ta–B–C coatings prepared by DCMS and HiPIMS co-sputtering. Vacuum. 2022;199:110937.